

Electronic Structures of Divinylchalcogenophene-Bridged Biruthenium Complexes: Exploring Trends from O to Te

Wen-Xia Liu,^[a] Feng Yan,^[a] Shu-Li Qian,^[a] Jin-Yu Ye,^[b] Xu Liu,^[a] Ming-Xia Yu,^[a] Xiao-Hui Wu,^[a] Meng-Lei Le,^[a] Zhi-You Zhou,^[b] Sheng-Hua Liu,^[a] Paul J. Low^{*[c]} and Shan Jin^{*[a]}

Abstract: An homologous series of divinylchalcogenophene-bridged binuclear ruthenium complexes $[(PMe_3)_3Cl(CO)Ru]_2(\mu-CH=CH-C_4H_2X-CH=CH)$ (**4a-4d**, X = O, S, Se, Te) has been synthesized and fully characterized by X-ray crystallography and various spectroscopic techniques. Single-crystal X-ray diffraction results show a distinct short-long bond length alternation along the polyene-like hydrocarbon backbone, with the geometric constraints imposed by the chalcogenophene leading to an increasing distance between two metal centres (d_{Ru-Ru}) in complexes **4a-4d** as the heteroatom in the five-membered ring is changed from oxygen (9.980 Å in **4a**) to tellurium (11.063 Å in **4d**). The complexes undergo two sequential one-electron oxidation processes, the half-wave potential and separation of which appear to be sensitive to a range of factors including aromatic stabilization and reorganization energies. Analysis of $[4a-4d]^{n+}$ ($n = 0, 1, 2$) by UV-Vis-NIR and IR spectroelectrochemical methods, supported by DFT calculations ($n = 0, 1$) revealed that the redox character of the complexes is dominated by the polyene-like backbone, with the chalcogenide playing a subtle but influential, structural rather than electronic, role. In the radical cations $[4a-4d]^+$, charge is rather effectively delocalized over the 10-atom Ru-{4-*s-cis*-all-*trans*-(CH=CH)₄}-Ru chain, giving rise to a species with spectroscopic properties not dissimilar to oxidized polyacetylene.

Introduction

Since the initial explorations of the Creutz-Taube ion in 1969^[1] there has been intense interest in the electronic structures, redox properties and electron transfer characteristics of compounds and complexes in which two (or more) organic, organometallic or inorganic electrophores are linked through a common bridge.^[2-8] Such studies underpin both our fundamental understanding of intramolecular electron transfer processes, and are further motivated by interest in modeling electron transfer processes in biology and for the design of advanced optoelectronic materials. In this regard, bimetallic complexes $[L_nM(\mu\text{-bridge})ML_n]$, in which two ostensibly redox-active metal centres M supported by auxiliary ligands L are linked by a π -conjugated bridging unit, have attracted considerable attention.^[3,9-14] Consequently, bimetallic complexes featuring a wide variety of metal end-caps and π -conjugated bridges, including carbon-rich chains such as oligoynyl,^[15-37] oligoenyl,^[38-41] aromatic hydrocarbons^[42-50] and heterocycles,^[51,52] bridging ligands containing other main group elements,^[53-57] carboranes,^[58] and even other metal units,^[59-63] have been prepared and studied.

Most commonly, electron transfer within these bimetallic assemblies is not assessed directly from the $[L_nM(\mu\text{-bridge})ML_n]$ species, but rather from analysis of the 'inter-valence charge transfer' (IVCT) absorption band found in the 'mixed-valence' derivatives $[L_nM(\mu\text{-bridge})ML_n]^+$, with the electronic coupling between the

metal centres, H_{ab} , being determined by analysis of the IVCT band-shape within the framework of Marcus-Hush theory and its variations.^[3,5-7] However, it is increasingly recognized that many $[L_nM(\mu\text{-bridge})ML_n]^+$ systems are better described in terms of bridge-based redox character than metal-based mixed-valency.^[9,11,42,44,45,64]

Consequently, depending on the nature of the interactions between the metal centres and the bridging ligand, $[L_nM(\mu\text{-bridge})ML_n]^+$ systems can serve as models through which to probe bridge-mediated electron-transfer within the mixed-valence regime, or serve as models through which to explore characteristics of the oxidized bridging ligand.

Within the broad-range of bridging ligands examined within $[L_nM(\mu\text{-bridge})ML_n]^+$ complexes, thiophene derivatives have attracted attention,^[36,65-72] with the lower aromaticity of the heterocyclic ring in comparison with benzene thought likely to lead to increased contributions from a cumulene-like ground state and more extensively delocalized electronic structures.^[73,74] For example, Lapinte and Lo Sterzo and their respective co-workers have reported that 2,5-diethynylthiophene-linked iron(II) $Fe(dppe)Cp^*$ and $Fe(dppe)Cp$ termini are more strongly coupled than in the 1,4-diethynylbenzene-bridged analogues.^[48,69] Many other bimetallic complexes and metallopolymers with 2,5-diethynylthiophene-based bridging ligands are also known to offer highly delocalized electronic structures with significant contributions from the bridging ligand to the frontier molecular orbitals.^[36,49,65,75-83]

Against this backdrop of long-standing interest in the properties of bimetallic complexes featuring (oligo)thiophene-based bridges, there has been increasing interest in genuine mixed-valence compounds featuring oligofuran-based bridging ligands.^[84-87] Gidron and Bendikov reported that oligofurans can offer stronger electronic coupling between ferrocenyl redox units than oligothiophenes.^[84] Similar results have also been confirmed by Lang et al. using ruthenium or iron (II) complexes as redox-active termini bridged by 2,5-diethynylfuran and 2,5-diethynylthiophene.^[85,86] However, in 2,5-diethynylfuran and 2,5-diethynylthiophene bridged bis(ferrocene) complexes the thiophene derivative is likely modestly more strongly coupled.^[88] Unsurprisingly it can therefore be concluded that the electronic structures and degree of bridge-mediated electronic interactions in these systems are sensitive to both the heteroatom and the nature of the metal complex-bridge link. Despite the extensive explorations of thiophene-based bridging ligands, and the potential for tuning the electronic structure of the resulting complexes through the nature of the heteroatom demonstrated by these few comparative studies with furan-based analogues, selenophene and tellurophene containing bridging ligands have received little attention,^[89,90] and systematic studies of the influence of the full chalcogenophene series on the electronic structures of bimetallic complexes $[ML_n(\mu\text{-bridge})ML_n]^+$ are scarce.

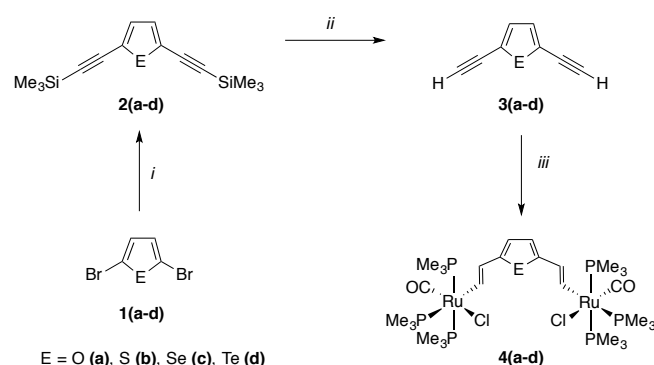
In designing a study to explore electronic structure and electron-transfer processes in mixed-valence $[ML_n(\mu\text{-bridge})ML_n]^+$ complexes there is considerable advantage in looking beyond traditional methods of analysis based on IVCT band-shape.^[3] As is now well-documented, the IVCT band is often overlapped with other low-energy electronic transitions,^[7,31,58] whilst different thermally-accessible molecular conformers in solution lead to a distribution of metal-bridge orbital overlaps, and hence a range of electronic coupling characteristics and multiple 'IVCT' transitions.^[28,30,42,45] Accurate interpretation of the resulting heavily overlapped and poorly resolved optical absorption band envelopes is challenging. Increasingly evidence from other spectroscopic methods with a range of timescales (e.g. IR, EPR, Mössbauer)^[10,28-30,42,85,91-94] supported by computational studies^[8,12] is used to explore

the electronic structure of complexes $[L_nM(\mu\text{-bridge})ML_n]^+$, many of which do not conform well to the traditional interpretations based on metal-based redox processes in static molecular structures.

Binuclear ruthenium mixed-valence complexes where two “ $RuCl(CO)(PR_3)_2L$ ” (L = neutral two-electron donor or free coordination site) redox-active termini are connected by a carbon-rich unsaturated spacer display well-behaved redox chemistry, and are ideally suited for studies of electron-density distribution and interplay between the properties of the bridge and metal centres, and charge transfer characteristics.^[40,44,47,64,86,95-97] In particular, the synergistic nature of the bonding interactions between the Ru metal centre and ancillary CO ligand result in the $\nu(CO)$ IR band being an excellent reporter group of metal electron density.^[46,98,99] With this in mind, we report here the synthesis, electrochemical behavior and spectroscopic characterization of a full series of chalcogenophene-bridged binuclear ruthenium complexes **4a-4d** (Scheme 1) with the aim of exploring their electronic structures as a function of the heteroatom (O, S, Se, Te) in the bridging ligand and redox state. The parent bimetallic complexes were fully characterized by NMR spectroscopy, X-ray diffraction, and elemental analysis, while the redox products were explored by UV-Vis-NIR and IR spectroelectrochemistry, supported by DFT calculations using the global hybrid BLYP35 functional.

Results and Discussion

Syntheses and Characterization. The divinylheterocyclic-bridged bimetallic ruthenium complexes **4a-4d** were synthesized as outlined in Scheme 1. In brief, the dibromides **1a-1d** were cross-coupled with trimethylsilylacetylene under Sonogashira conditions to give the bis(trimethylsilylethynyl) compounds **2a-2d**. Removal of the trimethylsilyl protecting groups (KOH/MeOH or $[n\text{-Bu}_4\text{N}]\text{F}$ (TBAF) /THF) gave the thermally and photochemically sensitive terminal alkynes **3a-3d** which were immediately reacted with the ruthenium hydride complex $[RuHCl(CO)(PPh_3)_3]$ to yield the hydridoruthenated products $[(PPh_3)_2Cl(CO)Ru]_2(\mu\text{-CH=CH-C}_4\text{H}_2\text{X-CH=CH})$ ($X = O, S, Se, Te$). As these five-coordinate complexes proved to be air-sensitive, especially in solution, the reaction mixture was directly treated with PMe_3 without further purification to give the corresponding six-coordinate products **4a-4d**.



Scheme 1. Synthesis of chalcogenophene-based bimetallic ruthenium complexes **4a-4d**. i) TMSA, $[PdCl_2(PPh_3)_2]$, CuI, THF/ Et_3N ; ii) KOH/MeOH (**4a-4c**) or TBAF/THF (**4d**); iii) $[RuHCl(CO)(PPh_3)_3]$, PMe_3 , CH_2Cl_2 (TMSA = trimethylsilyl acetylene, TBAF = tetra-*n*-butylammonium fluoride).

In the 1H NMR spectrum (in $CDCl_3$) of **4a-4d** the vinyl protons display two well-resolved doublets-of-multiplets near 7.2-7.8 ppm (Ru-CH) and 6.4-6.7 ppm (Ru-CH=CH), which are typical for *E*-Ru-CH=CH fragments of this type, albeit that the Ru-CH protons were shifted slightly upfield in comparison with those in complex $[RuCl(CO)(PMe_3)_3]_2(\mu\text{-CH=CH-C}_6\text{H}_5\text{-CH=CH})$ (**4e**).^[46] The two vinylic protons were

trans to each other over the double bond, due to the approach of the Ru-H to the same side of the alkyne moiety during the hydorruthenation reaction. The ^1H NMR and ^{13}C NMR spectra of **4a-4d** show a rather large downfield shift of the resonances arising from the chalcogenophene backbone from X = O to Te in line with the decreasing electronegativity of the chalcogenide.^[100,101] The geometry of the octatetraene-like hydrocarbon backbone was confirmed by the X-ray structures of **4a-4d** (Figure 1).

Molecular Structures. The furan-, thiophene-, selenophene- and tellurophene-bridged diruthenium vinyl complexes **4a-4d** were further characterized by single crystal X-ray diffraction analysis. In each case, suitable single crystals corresponding complex in dichloromethane at room temperature. The molecular structures of **4a-4d** are displayed in Figure 1. The crystallographic details are given in Tables S1 and S2 (Supporting Information). Selected bond lengths and angles for **4a-4d** are presented in Tables S3.

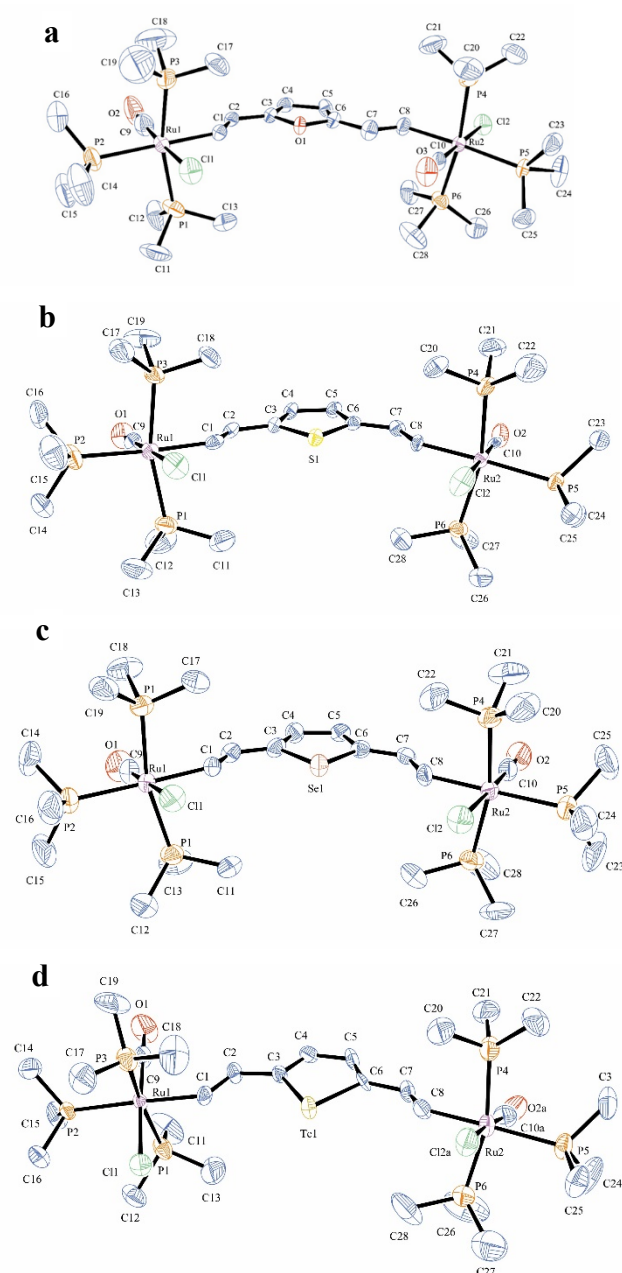


Figure 1. ORTEP diagrams (50% probability level) of the molecular structures of **4a-4d** (a-d) with the atom numbering scheme. Hydrogen atoms are omitted for clarity.

The structures of related bimetallic divinyl furan and thiophene ruthenium complexes have been recently reported.^[85,86] However, complexes **4a-4d** represent the first, crystallographically characterized example of a systemic chalcogenophene series of binuclear complexes (Figure 1). The linearly-conjugated complexes **4a-4d** consist of two {RuCl(CO)(PMe₃)₃} end-groups linked by a 2,5-divinyl substituted five-membered heterocycle carbon chain through Ru–C σ -bonding. In **4a**, the vinylic double bonds adopt *s-trans* and *s-cis* configurations around C(2)-C(3) and C(6)-C(7), respectively. The vinylic double bonds are both in *s-trans* configuration in **4b-4d** and directed towards the heteroatom. This is likely a combination of the well-documented electronic interactions that exist between the vinyl and CO moieties,^[102] possibly supported by a vinyl C-H...Cl interaction (Table S3).^[102-104] Whilst the significance of these secondary effects and the contribution that extended delocalization may play in stabilizing the observed structures cannot be readily deconvoluted, the carbon atoms of the μ -CH=CH-C₄H₂X-CH=CH (X = O, S, Se, Te) units are almost coplanar, with torsion angles between the core heterocycle ring and the two vinyl moieties of 176.9° for **4a**, 174.3° for **4b**, 176.2° for **4c**, and 173.8° for **4d** (Figure 1, Table S3).

The structures **4a-4d** display a number of trends that can be attributed to the changes in size and electronic characteristics of the chalcogenide. As the chalcogenide, E, becomes larger (O < S < Se < Te) the E-C(3) and E-C(6) bond lengths increase (Table S3). The decrease of the C(3)-E-C(6) bond angle is also a necessary consequence of the invariance of the bond length C(4)-C(5) and the increase of the bond lengths E-C(3) and E-C(6) down the row. This pulls atom E further away from the diene part of the heterocyclic ring, making the angle more acute. There is a distinct short-long alternation in C-C bond lengths along the C(1) to C(6) chain which follows the formal valence-bond description of these complexes shown in Scheme 1 with an octa-1,3,5,7-tetraene like structure along the hydrocarbon backbone. As a consequence of the structural changes at the chalcogenide, the C(3)-C(4)-C(5) and C(4)-C(5)-C(6) angles are forced wider, increasing from 105.3(7) and 108.2° (**4a**) to 118.0(9) and 120.2(1)° (**4d**). Consequently, the Ru1-Ru2 distances in complexes **4a-4d** increase upon changing the heteroatom of the five-membered ring from oxygen (9.980 Å in **4a**) to tellurium (11.063 Å in **4d**). In all cases, the Ru...Ru distances are significantly shorter than the corresponding value 11.901 Å in complex **4e**.^[46]

Bird has developed a simple parameter that provides a description of delocalisation in a cyclic system based on analysis of bond lengths.^[105] Higher values of the Bird index, *I*, correspond to more delocalized structures, with *I* = 100 representing a fully delocalized (aromatic) system. In the case of **4a-4d**, the Bird index, *I*, for the thiophene derivative **4b** (45.75) is somewhat higher than for the other members of the series (**4a** (27.52); **4c** (30.49); **4d** (26.88)), and on this basis, **4b** presents the most delocalized ground state structure.

Electrochemistry: The redox behavior of complexes **4a-4d** (1 mM in CH₂Cl₂) has been investigated by cyclic voltammetry and square-wave voltammetry (SWV) using 0.05 M [n-Bu₄N][B(C₆F₅)₄] as supporting electrolyte. Voltammograms of complexes **4a-4d** are shown in Figure 2, whilst that of the reference compound [RuCl(CO)(PMe₃)₃]₂(μ -CH=CH-C₆H₅-CH=CH) (**4e**) is given in Figure S1. The electrochemical parameters are compiled in Table 1.

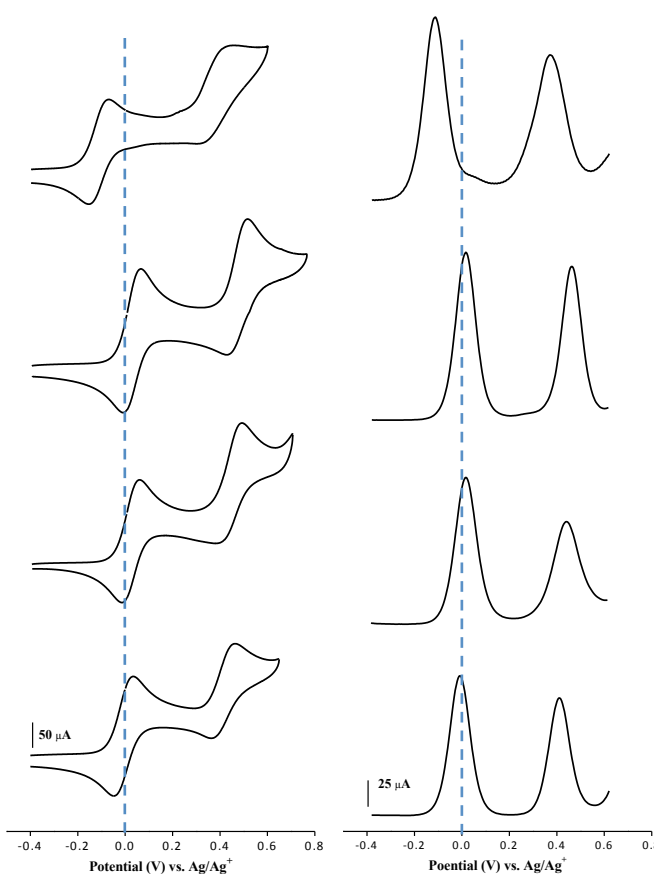


Figure 2. Cyclic voltammograms (CV) of complexes **4a-4d** (up to down) in $\text{CH}_2\text{Cl}_2/\text{n-Bu}_4\text{NB}(\text{C}_6\text{F}_5)_4$ at $\nu = 0.1 \text{ V s}^{-1}$. Square-wave voltammograms (SWV) at $f = 10 \text{ Hz}$. Potentials are given relative to the $\text{Ag}|\text{Ag}^+$ reference couple.

Table 1. Summary of electrochemical properties of **4a – 4e**.

	E_1 (V) <i>a</i>	E_2 (V) <i>a</i>	ΔE (mV) <i>b</i>	K_c ^c
4a	-0.114	0.374	488	1.78×10^8
4b	0.022	0.470	448	3.75×10^7
4c	0.016	0.440	424	1.47×10^7
4d	-0.007	0.413	420	1.26×10^7
4e <i>d</i>	0.260	0.610	348	7.64×10^5

^a From square-wave voltammetry in 0.05 M $[\text{n-Bu}_4\text{N}][\text{B}(\text{C}_6\text{F}_5)_4] / \text{CH}_2\text{Cl}_2$ solutions at 10 Hz for SWV. Potentials E_p are in V vs Ag^+/Ag ; under our conditions the Fc/Fc^+ couple exhibited $i_{pc}/i_{pa} = 0.99$, $\Delta E_p = 70 \text{ mV}$ and $E_{1/2}(\text{Fc}/\text{Fc}^+) = +0.22 \text{ V vs Ag}/\text{Ag}^+$. ^b Peak potential differences $\Delta E = E_2 - E_1$ are in mV. ^c The comproportionation constants, K_c , were calculated according to the formula $K_c = \exp(\Delta E/25.69)$ at 298 K. ^d Data from reference 46.

Complexes **4a-4d** displayed two consecutive one-electron redox processes in the potential range between -0.30 and 0.60 V vs. Ag^+/Ag the first being reversible, the second partially chemically reversible (Figure S2, Table S4). The first oxidation of the thiophene-bridged complex **4b** may also reflect the higher aromaticity of the thiophene moiety and the increased reorganisation energy associated with an

oxidation process based on the bridge, although there is no clear trend across the series (Table 1). The peak separation of the two redox waves ($\Delta E = E_2 - E_1$) decreases somewhat along the chalcogenophene series, ranging from 488 mV for the furan-bridged **4a** to 420 mV for tellurophene-bridged **4d** (Table 1). The corresponding comproportionation constants (K_c) range from 2×10^8 (**4a**) to 1×10^7 (**4d**). The ΔE and K_c values of **4a-4d** are considerably greater than those obtained for phenylene analogue **4e** (348 mV, $K_c = 7.64 \times 10^5$ in **4e**), and overall the large values of K_c demonstrate the significant thermodynamic stability of the one-electron oxidation products [**4a-4d**]⁺.^[9,106]

To further investigate the influence of the heteroatom (O, S, Se, Te) on the redox properties and electronic structure of complexes **4a-4d**, the UV-Vis-NIR and IR spectra of each member of the series in their various electrochemically accessible oxidation states were measured using spectroelectrochemical methods from solutions in CH₂Cl₂, containing 0.05 M [n-Bu₄N][B(C₆F₅)₄] as the supporting electrolyte.

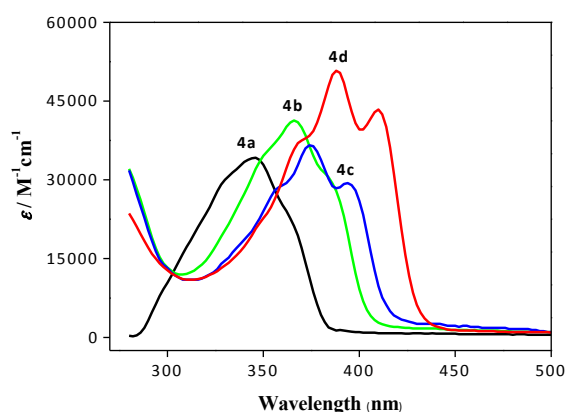


Figure 3. UV-Vis electronic absorption spectra of compounds **4a-4d** (1×10^{-5} M) in CH₂Cl₂.

UV-Vis-NIR spectroscopy and spectroelectrochemistry: The UV absorption spectra of the full series of binuclear chalcogenophene-bridged complexes **4a-4d** were measured in dichloromethane. The electronic absorption spectra (Figure 3, Table 2) show that the absorption maximum (λ_{\max}) of the band envelope shifts to longer wavelengths from X = O to S to Se to Te, indicating a decrease in the magnitude of the optical gap, a phenomenon also observed in the parent chalcogenophenes (Figure S2), and likely tracking the HOMO-LUMO gap. For **4a-4b**, the main broad transition envelopes in the near UV region are expected to arise from ligand-centred $\pi-\pi^*$ transitions of the chalcogenophene-core as the energy and fine-structure of these absorption features closely resemble those in the corresponding 2,5-bis(trimethylsilylethynyl)-substituted heterocycles **2a-2d** (Figure S3).

Table 2. UV-Vis adsorption properties of complexes **4a-4e** (1×10^{-5} M) in CH₂Cl₂ at 298 K.

	$\lambda_{\max} /$ nm, (eV) ^a	$\epsilon \times 10^{-4} /$ dm ³ ·mol ⁻¹ · cm ⁻¹	$\lambda_{\max} /$ nm (eV) (calculated) assignment	$D(H-L)$ (eV) ^b
4	348	3.12	328 (3.76)	4.87 ^c
a	(3.57) 368	0.79	HOMO- (LUMO+2)	

	(3.38)		(94%)	
4	370	1.72	350 (3.53)	4.76
b	(3.36)	1.33	HOMO-LUMO	
	388		(96%)	
	(3.20)			
4	378	1.14	361 (3.43)	4.64
c	(3.29)	1.84	HOMO-LUMO	
	397		(97%)	
	(3.13)			
4	389	3.01	366 (3.38)	4.58
d	(3.19)	3.38	HOMO-LUMO	
	411		(68%)	
	(3.02)		HOMO-	
			(LUMO+1)	
			(25%)	

^a Spectroscopic data from deconvolution of the UV spectra. ^b HOMO-LUMO energy gap. ^c D(HOMO-(LUMO+2)) = 5.04 eV

In order to gain insight into the oxidation products derived from the series of complexes **4a-4d**, UV-Vis-NIR spectroelectrochemical experiments were carried out in an optically transparent thin-layer electrochemical (OTTLE) cell with 0.05 M [n-Bu₄N][B(C₆F₅)₄] as the supporting electrolyte and 2.0 mmol·L⁻¹ of **4a-4d** at 25 °C. Upon one-electron oxidation of complexes **4a-4d** to [**4a-4d**]⁺, the π-π* bands shift from the UV region into the visible region (450-650 nm for [**4a**]⁺ and 500-750 nm for [**4b-4d**]⁺). In addition, [**4b-4d**]⁺ show intense absorption bands in the NIR region between 750 and 1300 nm (Figure 4), similar to those observed for both the radical complexes [(PⁱPr₃)₂(CO)ClRu]₂(μ-CH=CH-C₄H₂X-CH=CH)⁺ (X = O, S),^[86] in which the unpaired electron is delocalized along the molecular backbones, and the higher energy absorption band of hole-doped polyacetylene.^[107] The energy of these electronic absorption bands are essentially solvent independent (Figure S4), strongly supporting their assignment to transitions within a delocalised framework. With further oxidation to dicationic [**4a-4d**]²⁺ both absorption envelopes associated with the radical cations collapse and only higher energy bands characteristic of the π-π* transitions a closed-shell system are observed.

As noted above, for genuinely ‘mixed-valence’ complexes the band-shape of the intervalence charge transfer (IVCT) band can be used to provide details of the underlying electronic structure according to the generalized Marcus–Hush and Mulliken–Hush theories.^[3] However, the complications associated with such band-shape analysis are being increasingly recognised. Many MV complexes feature complex, low-energy absorption envelopes due to the multiple intervalence charge transfer (IVCT) processes, each of which may feature superposed vibrational progressions, or overlap with interconfigurational *d-d* transitions localised at the individual metal sites.^[7] In addition, many real molecular systems exist in solution not as a static lowest energy structure, but rather as a mixture of thermally populated conformers, each with their own electronic characteristics and absorption spectra which further complicate the appearance of electronic absorption bands and traditional methods of analysis,^[28,30,42,45] However, for comparison with the many examples of [L_nM(μ-bridge)ML_n]⁺ complexes in the literature with highly delocalised

electronic structures with significant bridge character that have been analysed within the framework of the Marcus-Hush model, key parameters are summarised in Table S5.

IR spectroscopy and spectroelectrochemistry: Infra-red spectroscopy can provide complementary information to that contained within the electronic absorption bands, and since IR bands are typically sharper and better resolved than the absorption envelopes associated with electronic transitions, IR spectroscopy can provide additional information concerning electron (de)localisation over the molecular framework.^[52,92,94,108,109] Thus for the most commonly studied $[L_nM(\mu\text{-bridge})ML_n]^+$ systems in which both metal centres and their ancillary ligands are identical, vibrational modes associated with symmetric atomic displacements of the bridge gain intensity in localised mixed-valence complexes due to the induced dipole over the entire molecule. In cases where suitable IR active vibrations associated with the metal fragments can be observed, information concerning the metal oxidation state(s) can also be obtained.^[93,95]

To further probe the nature of the redox products, *in situ* IR difference spectra studies were carried out on complexes **4a-4d** during electrochemical oxidation. The $\nu(\text{CO})$ bands were monitored to elucidate the nature of changes in molecular and electronic structure of the $(\text{CH}=\text{CH})\text{Ru}(\text{CO})\text{Cl}(\text{PMe}_3)_3$ units in $[\mathbf{4a} - \mathbf{4d}]^{n+}$ ($n = 0, 1, 2$). The spectra so obtained are illustrated in Figure 5 and $\nu(\text{CO})$ frequencies are summarised in Table 4. Figure 5 shows a series of *in situ* IR transmission difference spectra in the range between 1700 and 2200 cm^{-1} recorded with a potential sweep from -0.30 to +0.60 V, with respect to the reference IR spectrum obtained at -0.30 V. At this potential, complexes **4a-4e** exists in the formal $\text{Ru}_2^{\text{II,II}}$ state, and hence the downward and upward peaks correspond to the formation and diminishment of species, respectively. As shown in Figure 5, Figure S5, and Table 4, the $\nu(\text{CO})$ spectra of **4a – 4d** are essentially identical (1919 – 1921 cm^{-1}) and indicate similar electronic environments at the ruthenium centre in each case, despite the change in electronegativity of the chalcogenide.

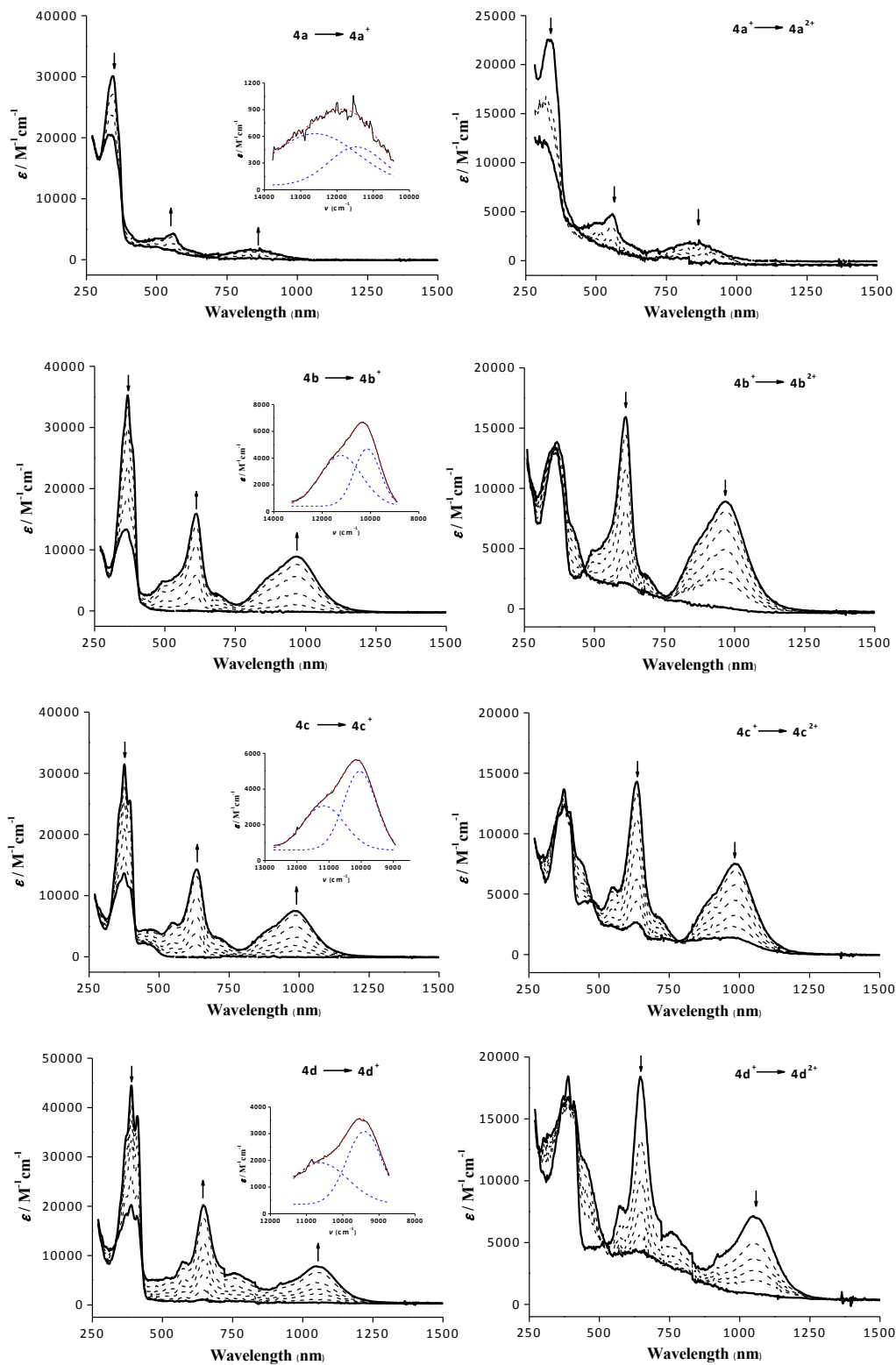


Figure 4. UV-vis-NIR spectra of complexes **4a-4d** collected during in situ oxidation in a spectroelectrochemical cell (Inset: Deconvoluted NIR spectra of $[4a-4d]^+$ in 0.05 M $CH_2Cl_2/n-Bu_4NB(C_6F_5)_4$. Black: experimental spectrum, blue: deconvoluted spectrum fitted with two Gaussian-shaped sub-bands, red: sum of Gaussian sub-bands).

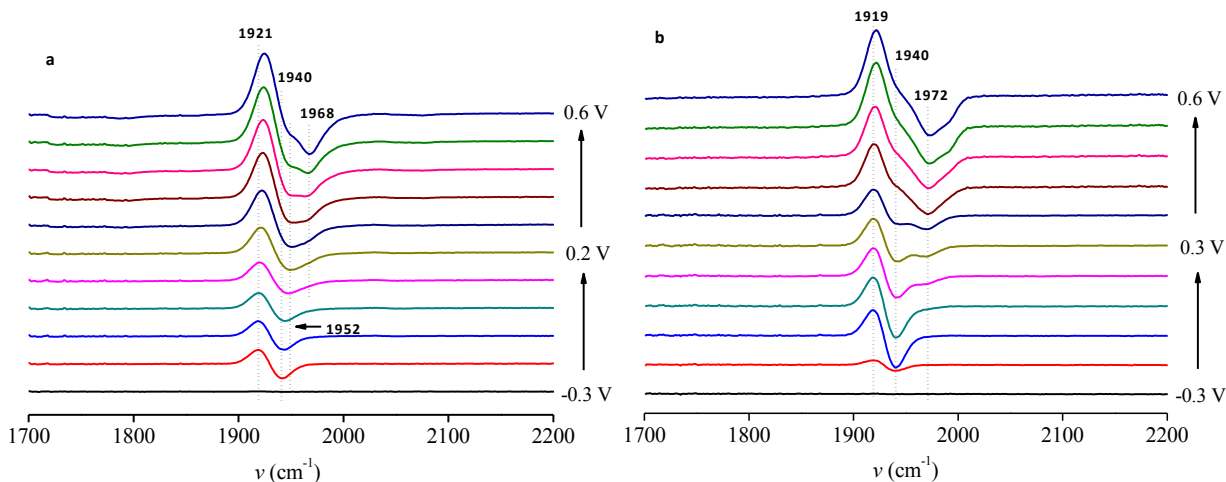


Figure 5. IR difference spectra of **4a** (a) and **4b** (b) recorded sequentially during a potential sweep from -0.30 → +0.60 V in a 0.05 M n-Bu₄NB(C₆F₅)₄-CH₂Cl₂ solution at 298K. The band 1952 cm⁻¹ associated with spectra of [**4a**]²⁺ cannot be assigned with confidence due to the poor chemical stability of **4a**²⁺.

Upon one-electron oxidation, the $\nu(\text{CO})$ band at 1919-1921 cm⁻¹ shifts to higher frequency by only ca. +20 cm⁻¹. During the second oxidation to the dications [**4a** – **4d**]²⁺, the $\nu(\text{CO})$ band undergoes a second shift to higher frequency by ca. +30 cm⁻¹. The small $\nu(\text{CO})$ shift indicates little change in the metal oxidation state accompanies the oxidation process, whilst the lack of any discernable splitting of the $\nu(\text{CO})$ band envelope is consistent with an equal electronic environment at the two metal centres on the IR timescale (ca. 10⁻¹³ s) in all three oxidation states.^[46,95] Together these observations strongly support the conclusions drawn from the UV-vis-NIR studies and descriptions of [**4a** – **4d**]⁺ in terms of a bridge-based oxidation

Table 4. Experimental (and computational)^a IR data $\nu(\text{CO}, \text{cm}^{-1})$ for complexes [**4a-4d**]ⁿ⁺ (n = 0, 1, 2) in their various oxidation states.

	4a	4b	4c	4d
0	1921 (1944)	1919 (1946)	1920 (1945)	1919 (1946)
1	1940 (1961)	1940 (1963)	1941 (1965)	1941 (1965)
2	1968 ^b	1972	1971	1968

^a corrected by a factor of 0.95.^[110]

Quantum chemical calculations: To gain further insight concerning the influence of the chalcogenide on the electronic structure of **4a** – **4d**, attention was turned to DFT calculations using the BLYP35 functional (*Gaussian 09*, LANL2DZ for Ru, Se and Te, 6-31G** for all other atoms, COSMO(CH₂Cl₂)).^[8,111,112] The 35% direct exchange contribution in the BLYP35 global hybrid functional has proved to be well-suited in the study of both localised and delocalised organic and organometallic mixed-valence complexes.^[113-119] Structures were optimized without constraints, and shown to be true minima by frequency analysis. The geometry optimisation consistently returned the all-*trans*-4-*s-cis* structures determined crystallographically for **4b** – **4d**, and no minimum structure corresponding to the all-*trans*-2-*s-trans*-4-*s-cis* conformation in the crystal structure of **4a** could be identified. It is likely that the

conformation adopted by **4a** in the crystal is a consequence of the solid state and packing phenomena

Important bond lengths and angles from the optimised geometries are summarised in Table S3, together with the equivalent parameters from the crystallographically determined structures for comparison. The Ru-P and Ru-Cl bond lengths are modestly over-estimated, but there is excellent correlation between the experimentally determined and calculated distances and angles along the Ru-(CH=CH)₄-Ru chain and for the parameters around the chalcogenide element. The accuracy of the computational models is further verified by the calculated $\nu(\text{CO})$ frequencies (Table 4). In each case the symmetric and asymmetric $\nu(\text{CO})$ stretching modes differ by only ca. 1 cm^{-1} and across the series fall within the small range of $1944 - 1946\text{ cm}^{-1}$, close to the experimental values of $1919 - 1920\text{ cm}^{-1}$.

Plots the HOMO and LUMO of **4a - 4d** together with the LUMO+2 of **4a** and LUMO+1 of **4d** are given in Figure 6, with a summary of the orbital composition in Table S6. The electronic structures are rather similar, despite the changes in the nature of the chalcogenide. At the level of theory employed, the HOMOs feature only 10% Ru character (5% from each metal atom), and no appreciable contributions from the chalcogenide. Rather, the composition and nodal properties of the HOMOs closely resemble those of the HOMO (or 4π MO with three nodal planes) of the 4-*s-cis*-all-*trans*-octatetraene-like fragment (85-87%) (Figure 6, Table S6). The LUMO of **4b - 4d** resembles the octatetraene-like π^* -manifold, with a small (6-8%) contribution from a chalcogenide p-type orbital. In the case of **4a**, the O atom contribution lifts the π^* system above low-lying empty metal d-orbitals, and becomes the LUMO+2. The HOMO-LUMO energy gap (or the similarly composed HOMO-(LUMO+2) for **4a**) displays the same trend as the lowest energy optical absorption over the series **4a - 4d**, progressively decreasing with the increasing atomic number of the chalcogenide, but these energies correlate only modestly with the energies of the lowest energy optical transitions (Table S6). TD-DFT calculations with a solvent model more accurately map the electronic absorption spectra of **4a - 4d** (Table 5). The lowest energy electronic absorptions of any appreciable intensity have octatetraene-like $\pi-\pi^*$ character, and arise from the HOMO-LUMO (or HOMO-(LUMO+2) in the case of **4a**) transitions. There is some admixed HOMO-(LUMO+1) character in the case of **4d**, which contributes more Te-character to the excited state.

The cation radicals were modelled at the same level of theory, with minima in the all-*trans*-4-*s-cis* conformation also being identified (Table S4). The calculated $\nu(\text{CO})$ frequencies of [**4a - 4d**]⁺ give rise to slightly greater differences in the symmetric and asymmetric stretches ($D\nu(\text{CO})$ ca. $2 - 3\text{ cm}^{-1}$) than in the neutral systems, but again these are too similar to be resolved in the $\nu(\text{CO})$ band envelope, which falls in the small range $1962 - 1966\text{ cm}^{-1}$. The ca. $+20\text{ cm}^{-1}$ shift of the $\nu(\text{CO})$ bands on oxidation is in excellent agreement with the experimental data (Table 4).

Close comparison of the molecular geometries reveals very small (ca. 0.02 \AA) contraction of the Ru-Cl bond lengths and a similar elongation of the Ru-P distances, indicating a small decrease in the electron density at the metal centre, consistent with the conclusions drawn from the computational vibrational and experimental IR spectra. The chalcogenide-C(3, 6) bond lengths are also insensitive to the change in molecular oxidation state (Table S3). More significant structure changes on oxidation are apparent along the 10-atom Ru-{4-*s-cis*-all-*trans*-(CH=CH)₄}-Ru chain, which adopts a less pronounced long-short bond length alternation. The C-C bond lengths

along the polyene-like chain differ by ca. 0.03 Å, consistent with more cumulene-like valence-bond structure.

The composition and nodal properties of the frontier orbitals in the radical cations [**4a** – **4d**]⁺ are similar to those described above than in the neutral systems, with the π* system in **4a**⁺ now descending below the empty metal d-orbitals (Figure 7). Thus the b-LUMO and a-HOMO of the radical cations both closely resemble the HOMOs of the neutral systems, whilst the a-LUMO is similar in structure to the LUMOs of the neutral systems. Therefore, to a good first approximation, the oxidation of **4a** – **4d** can be thought of in terms of depopulation of the HOMO, and the resulting radical cations offering similar electronic structure and characteristics as a conformationally well-defined fragment of oxidised polyacetylene.^[107] The lower-lying b-HOMO has appreciable metal-vinyl character, with increasingly important contributions from the chalcogenide along the series [**4a** – **4d**]⁺.

TD-DFT calculations have also been performed on [**4a** – **4d**]⁺ (Table S6). The calculations give two predominant transitions that correspond to the NIR and Vis absorption envelopes observed in the spectroelectrochemical experiments. The lowest energy transition of any appreciable oscillator strength has b-HOMO-b-LUMO character (>80%), and consideration of the composition of these orbitals allows the NIR band to be satisfactorily if approximately, attributed to a dπ-π transition. The higher energy transition which corresponds to the visible absorption envelope arises predominantly from the a-HOMO-a-LUMO transition and has the same π-π* character as the principle absorption feature in the neutral compounds. For **4d** the electronic description is somewhat more complex. The greater involvement of the Te atom in the composition of the b-HOMO lends a degree of TeLCT character to the NIR absorption band, whilst two transitions (588 nm, 546 nm) contribute to the higher energy band envelope, both offering b-(HOMO-5)-b-LUMO and a-HOMO-a-LUMO character (Table S6). Plots of the relevant orbitals from [**4a**]⁺ and [**4d**]⁺ are given in Figure 7 to illustrate these features. The limited metal contribution to the b-LUMO, coupled with the collapse of both the absorption band in the NIR region and the Visible absorption arising from the ligand-based π-π* on the second oxidation leads us to prefer a description of the radical cations [**4a** – **4d**]⁺ in terms of metal-supported oxidised oligoenes, rather than a formal description as Class III mixed-valence complexes.^[86]

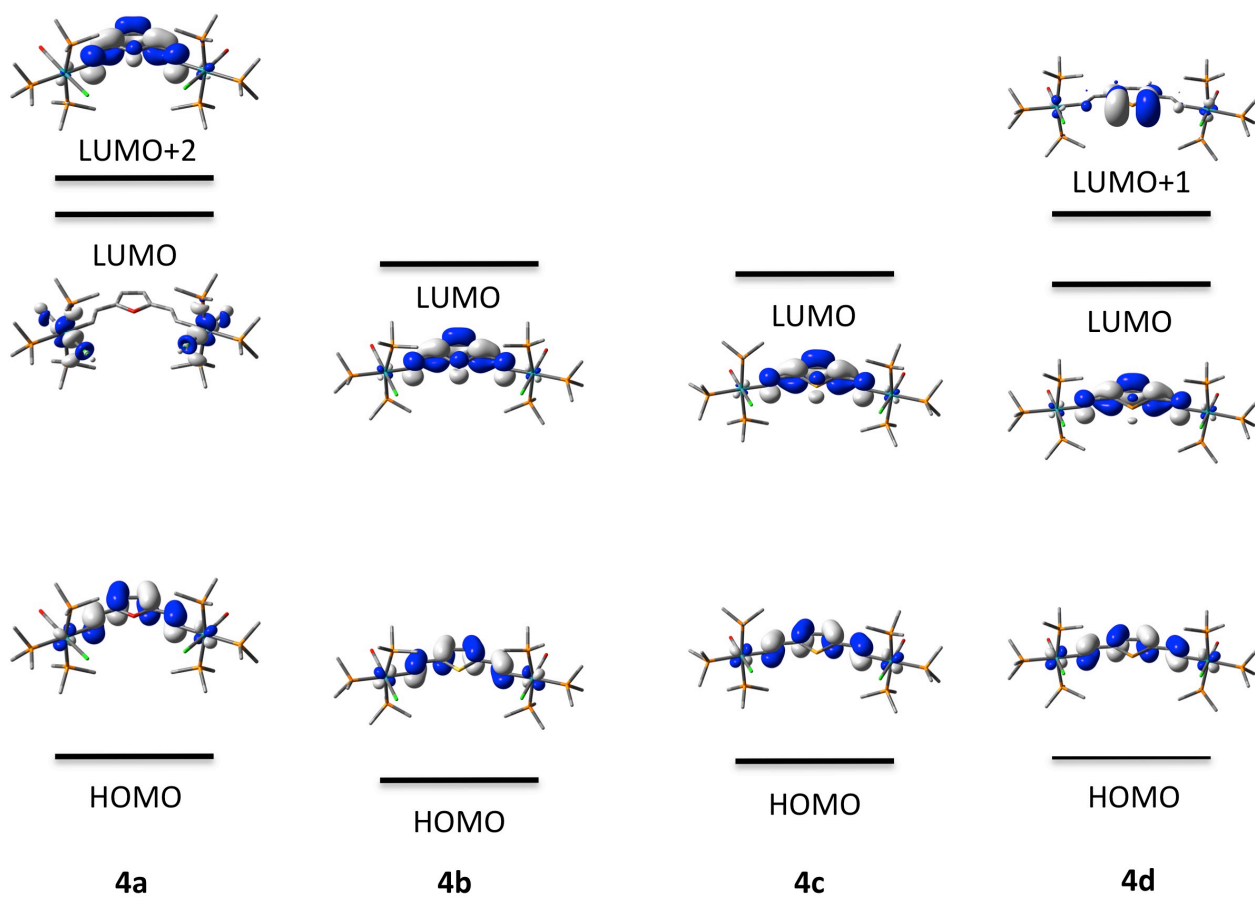


Figure 6. Plots of selected frontier MOs from 4a – 4d

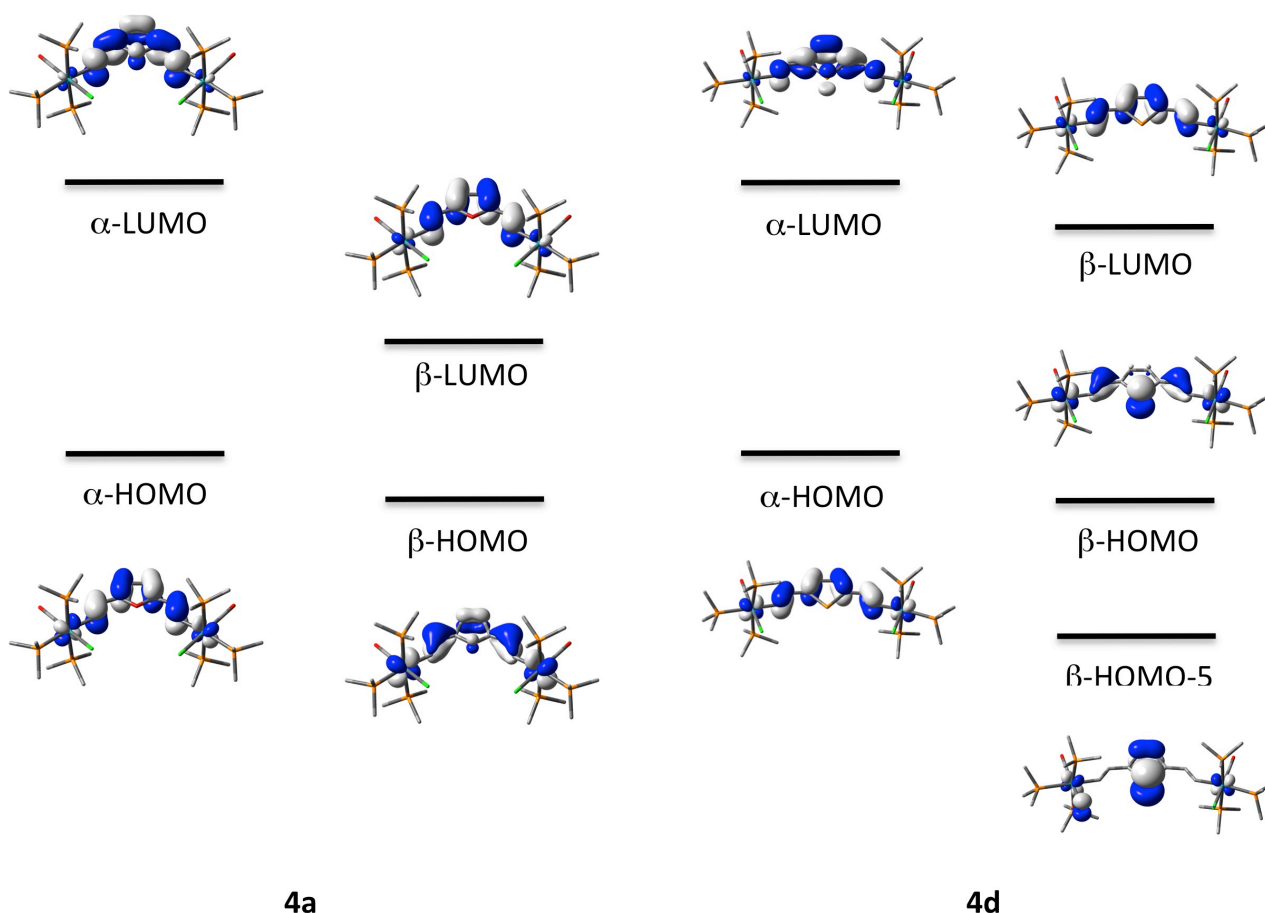


Figure 7. Plots of selected orbitals from $[4a]^+$ and $[4d]^+$.

Conclusions

A full series of divinylchalcogenophene-bridged binuclear ruthenium complexes $[(PMe_3)_3Cl(CO)Ru]_2(\mu-CH=CH-C_4H_2X-CH=CH)$ ($X = O, S, Se, Te$) has been reported with the aim of systematically studying any influence of the heteroatom on the electronic structure of these compounds and their redox-derived products. The first homologous series of chalcogenophene-bridged binuclear complexes **4a-4d** were completely characterized by single crystal X-ray diffraction analysis. The vinyl moieties and the five-membered heterocycles are almost coplanar to each other, allowing for extensive π -conjugation across the entire organometallic backbones. Single-crystal X-ray diffraction show that the Ru1-Ru2 distances in complexes **4a-4d** increase by changing the heteroatom of the five-membered ring from oxygen (**4a**) to tellurium (**4d**). The electronic absorption spectra of these compounds display an intense π - π^* transition associated with the conjugated 10-atom Ru- $\{4-s-cis-all-trans-(CH=CH)_4\}$ -Ru chain. The $\nu(CO)$ frequencies in the IR spectra were largely independent of the nature of the chalcogenide, consistent with the limited conjugation

of the metal-atoms to the chalcogenide. Rather, the metal-fragments serve as electron-donating capping groups to the oligoene. Oxidation of **4a** – **4d** to the radical cations **4a⁺**–**4d⁺** results in depopulation of the HOMO exhibit intense solvent-independent NIR absorption band-envelopes, arising from the b-HOMO-b-LUMO transition, whilst to higher energy the a-HOMO- a-LUMO transition retains the oligoene-like π - π^* character of the neutral systems. In turn, these and related systems provide further opportunities to model polarons of oxidised polyacetylene and other organic semi-conductors.

Experimental Section

General Materials. All manipulations were carried out at room temperature under an argon atmosphere using standard Schlenk techniques, unless otherwise stated. Solvents were predried, distilled, and degassed prior to use, except those for spectroscopic measurements, which were of spectroscopic grade. The reagents (trimethylsilyl)acetylene, selenophene, and 2,5-dibromothiophene (**1b**) were commercially available. The starting materials RuHCl(CO)(PPh₃)₃,^[120] tellurophene,^[90,121] 2,5-dibromofuran (**1a**),^[122] 2,5-dibromoselenophene (**1c**),^[123] 2,5-dibromotellurophene (**1d**),^[90] 2,5-bis(ethynyl)furan (**3a**),^[90] 2,5-bis(ethynyl)thiophene (**3b**),^[90] and [RuCl(CO)(PMe₃)₃]₂(μ -CH=CH-C₆H₄-CH=CH) (**4e**)^[46] were prepared by literature methods.

Synthesis of Bis(trimethylsilylethynyl) Heterocyclic Derivatives

2,5-Bis(trimethylsilylethynyl)furan (2a) (Trimethylsilyl)acetylene (0.49 g, 5 mmol) was added to a stirred solution of **1a** (0.226 g, 1 mmol), CuI (0.038 g, 0.2 mmol), and [Pd(PPh₃)₂Cl₂] (0.07 g, 0.1 mmol) in triethylamine (5 mL) and THF (10 mL) under an argon atmosphere, and the mixture was heated to reflux for 10 h at 60 °C. The cold solution was filtered through a bed of Celite. The filtrate was evaporated under reduced pressure and the residue was purified by silica-gel column chromatography (petroleum ether / dichloromethane = 5: 1) to give a pale yellow solid (0.25 g, 95%). ¹H NMR (400 MHz, CDCl₃): δ = 6.54 (s, 2H), 0.24 ppm (s, 18H).

2,5-Bis(trimethylsilylethynyl)thiophene (2b) The procedure of **2b** was similar to that for **2a**: **1b** (0.60 g, 2.5 mmol), CuI (0.095 g, 0.5 mmol), [Pd(PPh₃)₂Cl₂] (0.176 g, 0.25 mmol), triethylamine (5 mL), THF (10 mL), and (trimethylsilyl)acetylene (1.23 g, 12.5 mmol). Yield: 0.68 g (98%) of yellow solid. ¹H NMR (400 MHz, CDCl₃): δ = 7.04 (s, 2H), 0.24 ppm (s, 18H).

2,5-Bis(trimethylsilylethynyl)selenophene (2c) The procedure of **2c** was similar to that for **2a**: **1c** (0.29 g, 1 mmol), CuI (0.038 g, 0.2 mmol), [Pd(PPh₃)₂Cl₂] (0.070 g, 0.1 mmol), triethylamine (5 mL), THF (10 mL), and (trimethylsilyl)acetylene (0.49 g, 5 mmol). Yield: 0.29 g (90%) of yellow solid. ¹H NMR (400 MHz, CDCl₃): δ = 7.10 (s, 2H), 0.24 ppm (s, 18H).

2,5-Bis(trimethylsilylethynyl)tellurophene (2d) The procedure of **2d** was similar to that for **2a**: **1d** (0.34 g, 1 mmol), CuI (0.038 g, 0.2 mmol), [Pd(PPh₃)₂Cl₂] (0.070 g, 0.1 mmol), triethylamine (5 mL), THF (10 mL), and (trimethylsilyl)acetylene (0.49 g, 5 mmol). Yield: 0.19 g (50%) of yellow solid. ¹H NMR (400 MHz, CDCl₃): δ = 7.64 (s, 2H), 0.23 ppm (s, 18H).

Synthesis of Diethynyl Heterocyclic Derivatives

2,5-Bis(ethynyl)selenophene (3c) 2,5-Bis(trimethylsilylethynyl)selenophene **2c** (0.32 g, 1 mmol) was dissolved in methanol (30 mL). Aqueous potassium hydroxide (1 mL, 5 M) was added, and the reaction mixture was stirred at room temperature overnight.

The reaction mixture was diluted with pentane and washed with brine. The organic layer was dried over Na₂SO₄, and the solvent removed in vacuo, giving a yellow brown solid. Yield: 0.070 g (40%). ¹H NMR (400 MHz, CDCl₃): δ = 7.31(s, 2H), 3.54 ppm (s, 2H).

2,5-Bis(ethynyl)tellurophene (3d) 2,5-Bis(trimethylsilylethynyl) tellurophene **2d** (0.19 g, 0.5 mmol) was dissolved in THF (20 mL). TBAF (2.5 mL, 1 M) was added at -20 °C and stirred for 30 min, then the reaction mixture was stirred at room temperature overnight. The solution was filtered through a bed of Celite. The filtrate was evaporated under reduced pressure and the residue was purified by silica-gel column chromatography (pentane) to give a yellow solid. Yield: 0.050 g (44%). ¹H NMR (400 MHz, CDCl₃): δ = 7.72 (s, 2H), 3.72 ppm (s, 2H).

General Synthesis of Binuclear Ruthenium Complexes, 4a-4d

To a suspension of RuHCl(CO)(PPh₃)₃ (0.31 g, 0.33 mmol) in CH₂Cl₂ (20 mL) was slowly added a solution of the appropriate diethynyl heterocyclic compound **3a – 3d** (0.18 mmol) in CH₂Cl₂ (5 mL). The reaction mixture was stirred for 1h to give a red solution. Then a 1M THF solution of PMe₃ (1.8 mL, 1.8 mmol) was added to the red solution. The mixture was stirred for another 20 h. The solution was filtered through a column of Celite. The volume of the filtrate was reduced to ca. 2 mL under vacuum. Addition of hexane (6 mL) to the residue produced a solid, which was collected by filtration, washed with hexane, and dried under vacuum.

4a: Yield 0.090 g, 52%; ¹H NMR (400 MHz, CDCl₃): δ = 7.76-7.71 (m, 2H, Ru-CH=), 6.46-6.42 (m, 2H, C₄H₂O-CH=), 5.97 (s, 2H, C₄H₂O), 1.46 (d, *J* = 6.7 Hz, 18H, PMe₃), 1.40 ppm (t, *J* = 3.4 Hz, 36H, PMe₃); ³¹P NMR (160 MHz, CDCl₃): δ = -8.68 (d, *J* = 23.3 Hz), -20.13 ppm (t, *J* = 23.2 Hz); ¹³C NMR (100 MHz, CDCl₃): δ = 201.86 (q, *J*(P,C) = 25.2, 13.1 Hz, CO), 162.55 (dt, *J*(P,C) = 77.7, 17.6 Hz, Ru-CH=), 154.37 (d, *J*(P,C) = 6.6 Hz, Ru-CH=CH), 124.93 (C-2/5), 100.76 (C-3/4), 20.18 (t, *J*(P,C) = 18.6 Hz, PMe₃), 16.75 ppm (dd, *J*(P,C) = 15.5 Hz, PMe₃). Anal. Calcd for C₂₈H₆₀Cl₂O₃P₆Ru₂: C, 37.22; H, 6.69. Found: C, 37.32; H, 7.01.

4b: Yield 0.080 g, 48%; ¹H NMR (400 MHz, CDCl₃): δ = 7.68-7.60 (m, 2H, Ru-CH=), 6.63-6.57 (m, 2H, C₄H₂S-CH=), 6.44 (s, 2H, C₄H₂S), 1.45 (d, *J* = 6.8 Hz, 18H, PMe₃), 1.40 ppm (t, *J* = 3.4 Hz, 36H, PMe₃); ³¹P NMR (160 MHz, CDCl₃): δ = -8.25 (d, *J* = 22.6 Hz), -19.74 ppm (t, *J* = 20.7 Hz); ¹³C NMR (100 MHz, CD₂Cl₂): δ = 202.26 (q, *J*(P,C) = 24.9, 12.4 Hz, CO), 164.58 (dt, *J*(P,C) = 76.0, 19.4 Hz, Ru-CH=), 145.54 (m, Ru-CH=CH) 129.02 (C-2/5), 118.08 (C-3/4), 20.25 (d, *J*(P,C) = 21.2 Hz, PMe₃), 16.94 ppm (t, *J*(P,C) = 16.0 Hz, PMe₃). Anal. Calcd for C₂₈H₆₀Cl₂O₂P₆Ru₂S: C, 36.57; H, 6.58. Found: C, 36.72; H, 6.62.

4c: Yield 0.070 g, 40%; ¹H NMR (400 MHz, CDCl₃): δ (ppm) 7.59-7.51 (m, 2H, Ru-CH=), 6.66-6.60 (m, 2H, C₄H₂Se-CH=), 6.55 (s, 2H, C₄H₂Se), 1.45 (d, *J* = 6.8 Hz, 18H, PMe₃), 1.40 (t, *J* = 3.4 Hz, 36H, PMe₃); ³¹P NMR (160 MHz, CDCl₃): δ = -8.36 (d, *J* = 22.7 Hz), -19.87 ppm (t, *J* = 22.0 Hz); ¹³C NMR (100 MHz, CD₂Cl₂): δ = 202.83 (q, *J*(P,C) = 24.4, 12.8 Hz, CO), 168.72 (dm, *J*(P,C) = 75.5, 17.8 Hz, Ru-CH=), 131.98 (C-2/5), 120.16 (C-3/4), 20.25 (d, *J*(P,C) = 20.9 Hz, PMe₃), 16.93 ppm (t, *J*(P,C) = 15.2 Hz, PMe₃). Anal. Calcd for C₂₈H₆₀Cl₂O₂P₆Ru₂Se: C, 34.79; H, 6.26. Found: C, 34.63; H, 6.67.

4d: Yield 0.090 g, 49%; ¹H NMR (400 MHz, CDCl₃): δ = 7.34-7.27 (m, 2H, Ru-CH=), 6.91 (s, 2H, C₄H₂Te), 6.56-6.50 (m, 2H, C₄H₂Te-CH=), 1.45 (d, *J* = 6.8 Hz, 18H, PMe₃), 1.39 ppm (t, *J* = 3.4 Hz, 36H, PMe₃); ³¹P NMR (160 MHz, CDCl₃): δ = -8.29 (d, *J* = 22.6 Hz), -19.82 ppm (t, *J* = 22.5 Hz); ¹³C NMR (100 MHz, CDCl₃): δ = 202.21 (q, *J*(P,C) = 24.8, 12.2 Hz, CO), 169.79 (t, *J*(P,C) = 78.3, 16.1 Hz, Ru-CH=), 149.72 (m, Ru-CH=CH), 136.15 (C-2/5), 127.26 (C-3/4), 20.09 (d, *J*(P,C) = 21.0 Hz,

PMe₃), 16.82 ppm (t, $J(\text{P,C}) = 15.2$ Hz, PMe₃). Anal. Calcd for C₂₈H₆₀Cl₂O₂P₆Ru₂Te: C, 33.12; H, 5.96. Found: C, 33.22; H, 6.08.

4e: Yield 0.26 g, 70 %; ¹H NMR (400 MHz, CDCl₃): $\delta = 7.99$ -7.93 (m, 2H, Ru-CH=), 7.25 (s, 2H, Ph-H), 6.56-6.50 (m, 2H, Ph-CH=), 1.45 (d, $J = 6.8$ Hz, 18H, PMe₃), 1.39 (t, $J = 3.2$ Hz, 36H, PMe₃); ³¹P NMR (160 MHz, CDCl₃): $\delta = -9.35$ (d, $J = 21.1$ Hz), -21.01 (t, $J = 21.1$ Hz); ¹³C NMR (150 MHz, CDCl₃): $\delta = 202.48$ (CO), 164.72 (t, $J(\text{P,C}) = 15.5$ Hz, Ru-CH=), 137.79 (m, Ru-CH=CH), 134.86 (C-2/5), 124.34 (C-3/4), 20.13 (d, $J(\text{P,C}) = 20.55$ Hz, PMe₃), 16.56 ppm (t, $J(\text{P,C}) = 15.2$ Hz, PMe₃).

Physical Measurements. Elemental analyses (C, H, N) were performed by Vario EIII CHNSO. ¹H, ¹³C {¹H}, and ³¹P {¹H} NMR spectra were collected on a Varian MERCURY Plus 400 spectrometer (400 MHz). ¹H, ¹³C NMR chemical shifts are relative to TMS, and ³¹P NMR chemical shifts are relative to 85% H₃PO₄. UV-Vis spectra were recorded on a PDA spectrophotometer by quartz cells with path length of 1.0 cm. The electrochemical measurements were performed on a CHI 660D potentiostat (CHI USA). A three-electrode one-compartment cell was used to analyse the solution of the compound and supporting electrolyte in dry CH₂Cl₂. Deaeration of the solution was achieved by argon bubbling through the solution for about 10 min. before measurement. A 500 μm diameter platinum disc working electrode, a platinum wire counter electrode, and an Ag|Ag⁺ reference electrode were used. The Ag|Ag⁺ reference electrode contained an internal solution of 0.01 mol.dm⁻³ AgNO₃ in acetonitrile and was incorporated to the cell with a salt bridge containing 0.05 mol.dm⁻³ [n-Bu₄N][B(C₆F₅)₄] in CH₂Cl₂. UV/Vis/NIR experiments were performed with an airtight optically transparent thin-layer electrochemical (OTTLE) cell equipped with a Pt minigrad working electrode and CaF₂ windows with a path length of 200 μm .^[124] The cell was positioned in the sample compartment of a Shimadzu UV-3600 UV/Vis/NIR spectrophotometer. *In situ* FTIR experiments were carried out with a Nexus 870 FTIR spectrometer (Nicolet) equipped with a liquid-nitrogen cooled MCT-A detector. A model 263 A potentiostat/galvanostat (EG&G) was used to control electrode potential. The *In situ* FTIR experiments were performed by using a purpose-designed reflection-absorption cell in N₂ saturated CH₂Cl₂ solution. The working electrode was a glassy carbon of 5 mm in diameter, the counter electrode was a platinum foil. The reference electrode (Ag/Ag⁺) was separated from the bulk of the solution by a fritted-glass bridge of low porosity, which contained the solvent/supporting electrolyte mixture. The IR spectra were collected in single beam mode at 2 cm⁻¹, and differential absorbance spectra were presented against the reference spectrum recorded immediately prior to the application of the potential. All electrochemical experiments were carried out under ambient conditions.

Quantum chemical studies: All calculations were carried out with the Gaussian 09 suite of programs^[125] using the BLYP35 functional,^[119] LANL2DZ basis set for Ru, Se and Te,^[126-128] and 6-31G** for all other atoms.^[129] A COSMO(CH₂Cl₂) solvent model was also employed.^[111] Crystallographically determined structures were used as a starting point for geometry optimisations, which were carried out without constraints. Structures were confirmed as true minima by the absence of imaginary frequencies. Molecular orbital analysis was undertaken using the GaussSum package.^[130]

Acknowledgements

The authors acknowledge financial support from National Natural Science Foundation of China (Nos. 21173094 and 21573086) and the self-determined research funds of CCNU from the colleges' basic research. P.J.L. acknowledges the award of an ARC

Future Fellowship from the Australian Research Council (FT120100073). The authors thank Dr. J. X. Yu (The University of Adelaide) for useful discussions.

Keywords: ruthenium • oligoene • chalcogenophene • spectroelectrochemistry • DFT

- [1] C. Creutz, H. Taube, *J. Am. Chem. Soc.* **1969**, *91*, 3988–3989.
- [2] A. Heckmann, C. Lambert, *Angew. Chem. Int. Ed.* **2012**, *51*, 326–392.
- [3] C. Creutz, *Prog. Inorg. Chem.* **1983**, *30*, 1–73.
- [4] J. P. Launay, *Coord. Chem. Rev.* **2013**, *257*, 1544–1554.
- [5] D. M. D'Alessandro, F. R. Keene, *Chem. Soc. Rev.* **2006**, *35*, 424–440.
- [6] B. S. Brunschwig, C. Creutz, N. Sutin, *Chem. Soc. Rev.* **2002**, *31*, 168–184.
- [7] K. D. Demadis, C. M. Hartshorn, T. J. Meyer, *Chem. Rev.* **2001**, *101*, 2655–2685.
- [8] M. Parthey, M. Kaupp, *Chem. Soc. Rev.* **2014**, *43*, 5067–5088.
- [9] R. F. Winter, *Organometallics* **2014**, *33*, 4517–4536.
- [10] J.-F. Halet, C. Lapinte, *Coord. Chem. Rev.* **2013**, *257*, 1584–1613.
- [11] P. J. Low, *Coord. Chem. Rev.* **2013**, *257*, 1507–1532.
- [12] K. Costuas, S. Rigaut, *Dalton Trans.* **2011**, *40*, 5643–5658.
- [13] M. I. Bruce, P. J. Low, Elsevier, **2004**, pp. 179–444.
- [14] S. Barlow, Dermot O'Hare, *Chem. Rev.* **1997**, *97*, 637–670.
- [15] Q. Zheng, J. C. Bohling, T. B. Peters, A. C. Frisch, F. Hampel, J. A. Gladysz, *Chem. Eur. J.* **2006**, *12*, 6486–6505.
- [16] W. Mohr, J. Stahl, F. Hampel, J. A. Gladysz, *Chem. Eur. J.* **2003**, *9*, 3324–3340.
- [17] W. Mohr, J. Stahl, F. Hampel, J. A. Gladysz, *Inorg. Chem.* **2001**, *40*, 3263–3264.
- [18] R. Dembinski, T. Bartik, B. Bartik, M. Jaeger, J. A. Gladysz, *J. Am. Chem. Soc.* **2000**, *122*, 810–822.
- [19] M. Brady, W. Weng, Y. Zhou, J. W. Seyler, A. J. Amoroso, A. M. Arif, M. Böhme, G. Frenking, J. A. Gladysz, *J. Am. Chem. Soc.* **1997**, *119*, 775–788.
- [20] H. Jiao, K. Costuas, J. A. Gladysz, J.-F. Halet, M. Guillemot, L. Toupet, F. Paul, C. Lapinte, *J. Am. Chem. Soc.* **2003**, *125*, 9511–9522.
- [21] A. Burgun, F. Gendron, C. J. Sumby, T. Roisnel, O. Cador, K. Costuas, J.-F. Halet, M. I. Bruce, C. Lapinte, *Organometallics* **2014**, *33*, 2613–2627.
- [22] M. I. Bruce, K. Costuas, T. Davin, B. G. Ellis, J.-F. Halet, C. Lapinte, P. J. Low, M. E. Smith, B. W. Skelton, L. Toupet, et al., *Organometallics* **2005**, *24*, 3864–3881.
- [23] F. Coat, F. Paul, C. Lapinte, L. Toupet, K. Costuas, J.-F. Halet, *J. Organomet. Chem.* **2003**, *683*, 368–378.
- [24] F. Paul, W. E. Meyer, L. Toupet, H. Jiao, J. A. Gladysz, C. Lapinte, *J. Am. Chem. Soc.* **2000**, *122*, 9405–9414.
- [25] M. Guillemot, L. Toupet, L. Toupet, C. Lapinte, C. Lapinte, *Organometallics* **1998**, *17*, 1928–1930.
- [26] N. N. Le, T. L. L. C, *J. Am. Chem. Soc.* **1995**, *117*, 7129–7138.
- [27] F. Coat, C. Lapinte, *Organometallics* **1996**, *15*, 477–479.
- [28] J. B. G. Gluyas, S. Gückel, M. Kaupp, P. J. Low, *Chem. Eur. J.* **2016**, *22*, 16138–16146.
- [29] J. B. G. Gluyas, A. N. Sobolev, E. G. Moore, P. J. Low, *Organometallics* **2015**, *34*, 3923–3926.
- [30] M. Parthey, J. B. G. Gluyas, P. A. Schauer, D. S. Yufit, J. A. K. Howard, M. Kaupp, P. J. Low, *Chem. Eur. J.* **2013**, *19*, 9780–9784.

- [31] E. C. Fitzgerald, N. J. Brown, R. Edge, M. Helliwell, H. N. Roberts, F. Tuna, A. Beeby, D. Collison, P. J. Low, M. W. Whiteley, *Organometallics* **2011**, *31*, 157–169.
- [32] M. I. Bruce, K. Costuas, T. Davin, J.-F. Halet, K. A. Kramarczuk, P. J. Low, B. K. Nicholson, G. J. Perkins, R. L. Roberts, B. W. Skelton, et al., *Dalton Trans.* **2007**, *33*, 5387.
- [33] M. I. Bruce, Benjamin G Ellis, P. J. Low, A. Brian W Skelton, A. H. White, *Organometallics* **2003**, *22*, 3184–3198.
- [34] M. I. Bruce, P. J. Low, K. Costuas, J.-F. Halet, S. P. Best, G. A. Heath, *J. Am. Chem. Soc.* **2000**, *122*, 1949–1962.
- [35] D.-B. Zhang, J.-Y. Wang, H.-M. Wen, Z.-N. Chen, *Organometallics* **2014**, *33*, 4738–4746.
- [36] L.-B. Gao, J. Kan, Y. Fan, L.-Y. Zhang, S. H. Liu, Z.-N. Chen, *Inorg. Chem.* **2007**, *46*, 5651–5664.
- [37] L.-B. Gao, L.-Y. Zhang, L.-X. Shi, Z.-N. Chen, *Organometallics* **2005**, *24*, 1678–1684.
- [38] S. H. Liu, H. Xia, T. B. Wen, Z. Zhou, G. Jia, *Organometallics* **2003**, *22*, 737–743.
- [39] S. H. Liu, Q. Y. Hu, P. Xue, T. B. Wen, I. D. Williams, G. Jia, *Organometallics* **2005**, *24*, 769–772.
- [40] J. Maurer, R. F. Winter, B. Sarkar, S. Záliš, *J Solid State Electrochem* **2005**, *9*, 738–749.
- [41] A.-C. Ribou, J.-P. Launay, M. L. Sachtleben, H. Li, C. W. Spangler, *Inorg. Chem.* **1996**, *35*, 3735–3740.
- [42] M. Parthey, J. B. G. Gluyas, M. A. Fox, P. J. Low, M. Kaupp, *Chem. Eur. J.* **2014**, *20*, 6895–6908.
- [43] J. Xia, Y.-P. Ou, Di Wu, G.-J. Jin, J. Yin, G.-A. Yu, S. H. Liu, *Dalton Trans.* **2013**, *42*, 14212–14222.
- [44] J.-L. Xia, W. Y. Man, X. Zhu, C. Zhang, G.-J. Jin, P. A. Schauer, M. A. Fox, J. Yin, G.-A. Yu, P. J. Low, et al., *Organometallics* **2012**, *31*, 5321–5333.
- [45] M. A. Fox, B. Le Guennic, R. L. Roberts, D. A. Brue, D. S. Yufit, J. A. K. Howard, G. Manca, J.-F. Halet, F. Hartl, P. J. Low, *J. Am. Chem. Soc.* **2011**, *133*, 18433–18446.
- [46] W. Y. Man, J.-L. Xia, N. J. Brown, J. D. Farmer, D. S. Yufit, J. A. K. Howard, S. H. Liu, P. J. Low, *Organometallics* **2011**, *30*, 1852–1858.
- [47] Y.-P. Ou, C. Jiang, D. Wu, J. Xia, J. Yin, S. Jin, G.-A. Yu, S. H. Liu, *Organometallics* **2011**, *30*, 5763–5770.
- [48] L. Medei, L. Orian, O. V. Semeikin, M. G. Peterleitner, N. A. Ustynyuk, S. Santi, C. Durante, A. Ricci, C. Lo Sterzo, *Chem. Ber.* **2006**, *2006*, 2582–2597.
- [49] M. C. B. Colbert, J. Lewis, N. J. Long, P. R. Raithby, M. Younus, A. J. P. White, D. J. Williams, N. N. Payne, L. Yellowlees, D. Beljonne, et al., *Organometallics* **1998**, *17*, 3034–3043.
- [50] N. Le Narvor, C. Lapinte, *Organometallics* **1995**, *14*, 634–639.
- [51] K. Costuas, O. Cador, F. Justaud, S. Le Stang, F. Paul, A. Monari, S. Evangelisti, L. Toupet, C. Lapinte, J.-F. Halet, *Inorg. Chem.* **2011**, *50*, 12601–12622.
- [52] T. Ito, T. Hamaguchi, H. Nagino, T. Yamaguchi, H. Kido, I. S. Zavarine, T. Richmond, J. Washington, C. P. Kubiak, *J. Am. Chem. Soc.* **1999**, *121*, 4625–4632.
- [53] G. Y. Zhu, M. Meng, Y. N. Tan, X. Xiao, C. Y. Liu, *Inorg. Chem.* **2016**, *55*, 6315–6322.
- [54] M. T. Kang, M. Meng, Y. N. Tan, T. Cheng, C. Y. Liu, *Chem. Eur. J.* **2016**, *22*, 3115–3126.

- [55] H. Lei, X. Xiao, M. Meng, T. Cheng, Y. Shu, Y. N. Tan, C. Y. Liu, *Inorg. Chim. Acta* **2015**, 424, 63–74.
- [56] M. E. Smith, E. L. Flynn, M. A. Fox, A. Trottier, E. Wrede, D. S. Yufit, J. A. K. Howard, K. L. Ronayne, M. Towrie, A. W. Parker, et al., *Chem. Commun.* **2008**, 5845–5847.
- [57] R. L. Cordiner, M. E. Smith, A. S. Batsanov, D. Albesa-Jové, F. Hartl, J. A. K. Howard, P. J. Low, *Inorg. Chim. Acta* **2006**, 359, 946–961.
- [58] N. J. Brown, H. N. Lancashire, M. A. Fox, D. Collison, R. Edge, D. S. Yufit, J. A. K. Howard, M. W. Whiteley, P. J. Low, *Organometallics* **2010**, 30, 884–894.
- [1] C. Creutz, H. Taube, *J. Am. Chem. Soc.* **1969**, 91, 3988–3989.
- [2] A. Heckmann, C. Lambert, *Angew. Chem. Int. Ed.* **2012**, 51, 326–392.
- [3] C. Creutz, *Prog. Inorg. Chem.* **1983**, 30, 1–73.
- [4] J. P. Launay, *Coord. Chem. Rev.* **2013**, 257, 1544–1554.
- [5] D. M. D'Alessandro, F. R. Keene, *Chem. Soc. Rev.* **2006**, 35, 424–440.
- [6] B. S. Brunshwig, C. Creutz, N. Sutin, *Chem. Soc. Rev.* **2002**, 31, 168–184.
- [7] K. D. Demadis, C. M. Hartshorn, T. J. Meyer, *Chem. Rev.* **2001**, 101, 2655–2685.
- [8] M. Parthey, M. Kaupp, *Chem. Soc. Rev.* **2014**, 43, 5067–5088.
- [9] R. F. Winter, *Organometallics* **2014**, 33, 4517–4536.
- [10] J.-F. Halet, C. Lapinte, *Coord. Chem. Rev.* **2013**, 257, 1584–1613.
- [11] P. J. Low, *Coord. Chem. Rev.* **2013**, 257, 1507–1532.
- [12] K. Costuas, S. Rigaut, *Dalton Trans.* **2011**, 40, 5643–5658.
- [13] M. I. Bruce, P. J. Low, Elsevier, **2004**, pp. 179–444.
- [14] S. Barlow, Dermot O'Hare, *Chem. Rev.* **1997**, 97, 637–670.
- [15] Q. Zheng, J. C. Bohling, T. B. Peters, A. C. Frisch, F. Hampel, J. A. Gladysz, *Chem. Eur. J.* **2006**, 12, 6486–6505.
- [16] W. Mohr, J. Stahl, F. Hampel, J. A. Gladysz, *Chem. Eur. J.* **2003**, 9, 3324–3340.
- [17] W. Mohr, J. Stahl, F. Hampel, J. A. Gladysz, *Inorg. Chem.* **2001**, 40, 3263–3264.
- [18] R. Dembinski, T. Bartik, B. Bartik, M. Jaeger, J. A. Gladysz, *J. Am. Chem. Soc.* **2000**, 122, 810–822.
- [19] M. Brady, W. Weng, Y. Zhou, J. W. Seyler, A. J. Amoroso, A. M. Arif, M. Böhme, G. Frenking, J. A. Gladysz, *J. Am. Chem. Soc.* **1997**, 119, 775–788.
- [20] H. Jiao, K. Costuas, J. A. Gladysz, J.-F. Halet, M. Guillemot, L. Toupet, F. Paul, C. Lapinte, *J. Am. Chem. Soc.* **2003**, 125, 9511–9522.
- [21] A. Burgun, F. Gendron, C. J. Sumbly, T. Roisnel, O. Cador, K. Costuas, J.-F. Halet, M. I. Bruce, C. Lapinte, *Organometallics* **2014**, 33, 2613–2627.
- [22] M. I. Bruce, K. Costuas, T. Davin, B. G. Ellis, J.-F. Halet, C. Lapinte, P. J. Low, M. E. Smith, B. W. Skelton, L. Toupet, et al., *Organometallics* **2005**, 24, 3864–3881.
- [23] F. Coat, F. Paul, C. Lapinte, L. Toupet, K. Costuas, J.-F. Halet, *J. Organomet. Chem.* **2003**, 683, 368–378.
- [24] F. Paul, W. E. Meyer, L. Toupet, H. Jiao, J. A. Gladysz, C. Lapinte, *J. Am. Chem. Soc.* **2000**, 122, 9405–9414.
- [25] M. Guillemot, L. Toupet, L. Toupet, C. Lapinte, C. Lapinte, *Organometallics* **1998**, 17, 1928–1930.
- [26] N. N. Le, T. L. C., *J. Am. Chem. Soc.* **1995**, 117, 7129–7138.
- [27] F. Coat, C. Lapinte, *Organometallics* **1996**, 15, 477–479.

- [28] J. B. G. Gluyas, S. Gückel, M. Kaupp, P. J. Low, *Chem. Eur. J.* **2016**, *22*, 16138–16146.
- [29] J. B. G. Gluyas, A. N. Sobolev, E. G. Moore, P. J. Low, *Organometallics* **2015**, *34*, 3923–3926.
- [30] M. Parthey, J. B. G. Gluyas, P. A. Schauer, D. S. Yufit, J. A. K. Howard, M. Kaupp, P. J. Low, *Chem. Eur. J.* **2013**, *19*, 9780–9784.
- [31] E. C. Fitzgerald, N. J. Brown, R. Edge, M. Helliwell, H. N. Roberts, F. Tuna, A. Beeby, D. Collison, P. J. Low, M. W. Whiteley, *Organometallics* **2011**, *31*, 157–169.
- [32] M. I. Bruce, K. Costuas, T. Davin, J.-F. Halet, K. A. Kramarczuk, P. J. Low, B. K. Nicholson, G. J. Perkins, R. L. Roberts, B. W. Skelton, et al., *Dalton Trans.* **2007**, *33*, 5387.
- [33] M. I. Bruce, Benjamin G Ellis, P. J. Low, A. Brian W Skelton, A. H. White, *Organometallics* **2003**, *22*, 3184–3198.
- [34] M. I. Bruce, P. J. Low, K. Costuas, J.-F. Halet, S. P. Best, G. A. Heath, *J. Am. Chem. Soc.* **2000**, *122*, 1949–1962.
- [35] D.-B. Zhang, J.-Y. Wang, H.-M. Wen, Z.-N. Chen, *Organometallics* **2014**, *33*, 4738–4746.
- [36] L.-B. Gao, J. Kan, Y. Fan, L.-Y. Zhang, S. H. Liu, Z.-N. Chen, *Inorg. Chem.* **2007**, *46*, 5651–5664.
- [37] L.-B. Gao, L.-Y. Zhang, L.-X. Shi, Z.-N. Chen, *Organometallics* **2005**, *24*, 1678–1684.
- [38] S. H. Liu, H. Xia, T. B. Wen, Z. Zhou, G. Jia, *Organometallics* **2003**, *22*, 737–743.
- [39] S. H. Liu, Q. Y. Hu, P. Xue, T. B. Wen, I. D. Williams, G. Jia, *Organometallics* **2005**, *24*, 769–772.
- [40] J. Maurer, R. F. Winter, B. Sarkar, S. Záliš, *J Solid State Electrochem* **2005**, *9*, 738–749.
- [41] A.-C. Ribou, J.-P. Launay, M. L. Sachtleben, H. Li, C. W. Spangler, *Inorg. Chem.* **1996**, *35*, 3735–3740.
- [42] M. Parthey, J. B. G. Gluyas, M. A. Fox, P. J. Low, M. Kaupp, *Chem. Eur. J.* **2014**, *20*, 6895–6908.
- [43] J. Xia, Y.-P. Ou, Di Wu, G.-J. Jin, J. Yin, G.-A. Yu, S. H. Liu, *Dalton Trans.* **2013**, *42*, 14212–14222.
- [44] J.-L. Xia, W. Y. Man, X. Zhu, C. Zhang, G.-J. Jin, P. A. Schauer, M. A. Fox, J. Yin, G.-A. Yu, P. J. Low, et al., *Organometallics* **2012**, *31*, 5321–5333.
- [45] M. A. Fox, B. Le Guennic, R. L. Roberts, D. A. Brue, D. S. Yufit, J. A. K. Howard, G. Manca, J.-F. Halet, F. Hartl, P. J. Low, *J. Am. Chem. Soc.* **2011**, *133*, 18433–18446.
- [46] W. Y. Man, J.-L. Xia, N. J. Brown, J. D. Farmer, D. S. Yufit, J. A. K. Howard, S. H. Liu, P. J. Low, *Organometallics* **2011**, *30*, 1852–1858.
- [47] Y.-P. Ou, C. Jiang, D. Wu, J. Xia, J. Yin, S. Jin, G.-A. Yu, S. H. Liu, *Organometallics* **2011**, *30*, 5763–5770.
- [48] L. Medei, L. Orian, O. V. Semeikin, M. G. Peterleitner, N. A. Ustynyuk, S. Santi, C. Durante, A. Ricci, C. Lo Sterzo, *Chem. Ber.* **2006**, *2006*, 2582–2597.
- [49] M. C. B. Colbert, J. Lewis, N. J. Long, P. R. Raithby, M. Younus, A. J. P. White, D. J. Williams, N. N. Payne, L. Yellowlees, D. Beljonne, et al., *Organometallics* **1998**, *17*, 3034–3043.
- [50] N. Le Narvor, C. Lapinte, *Organometallics* **1995**, *14*, 634–639.

- [51] K. Costuas, O. Cador, F. Justaud, S. Le Stang, F. Paul, A. Monari, S. Evangelisti, L. Toupet, C. Lapinte, J.-F. Halet, *Inorg. Chem.* **2011**, *50*, 12601–12622.
- [52] T. Ito, T. Hamaguchi, H. Nagino, T. Yamaguchi, H. Kido, I. S. Zavarine, T. Richmond, J. Washington, C. P. Kubiak, *J. Am. Chem. Soc.* **1999**, *121*, 4625–4632.
- [53] G. Y. Zhu, M. Meng, Y. N. Tan, X. Xiao, C. Y. Liu, *Inorg. Chem.* **2016**, *55*, 6315–6322.
- [54] M. T. Kang, M. Meng, Y. N. Tan, T. Cheng, C. Y. Liu, *Chem. Eur. J.* **2016**, *22*, 3115–3126.
- [55] H. Lei, X. Xiao, M. Meng, T. Cheng, Y. Shu, Y. N. Tan, C. Y. Liu, *Inorg. Chim. Acta* **2015**, *424*, 63–74.
- [56] M. E. Smith, E. L. Flynn, M. A. Fox, A. Trottier, E. Wrede, D. S. Yufit, J. A. K. Howard, K. L. Ronayne, M. Towrie, A. W. Parker, et al., *Chem. Commun.* **2008**, 5845–5847.
- [57] R. L. Cordiner, M. E. Smith, A. S. Batsanov, D. Albesa-Jové, F. Hartl, J. A. K. Howard, P. J. Low, *Inorg. Chim. Acta* **2006**, *359*, 946–961.
- [58] N. J. Brown, H. N. Lancashire, M. A. Fox, D. Collison, R. Edge, D. S. Yufit, J. A. K. Howard, M. W. Whiteley, P. J. Low, *Organometallics* **2010**, *30*, 884–894.
- [59] X. Ma, C. S. Lin, X. Q. Zhu, S. M. Hu, T. L. Sheng, X. T. Wu, *Angew. Chem. Int. Ed.* **2017**, *56*, 1605–1609.
- [60] F. Lissel, T. Fox, O. Blacque, W. Polit, R. F. Winter, K. Venkatesan, H. Berke, *J. Am. Chem. Soc.* **2013**, *135*, 4051–4060.
- [61] E. Wuttke, Y. M. Hervault, W. Polit, M. Linseis, P. Erler, S. Rigaut, R. F. Winter, *Organometallics* **2014**, *33*, 4672–4686.
- [62] J. B. G. Gluyas, A. J. Boden, S. G. Eaves, H. Yu, P. J. Low, *Dalton Trans.* **2014**, *43*, 6291–6294.
- [63] M. I. Bruce, B. Le Guennic, N. Scoleri, N. N. Zaitseva, J.-F. Halet, *Organometallics* **2012**, *31*, 4701–4706.
- [64] Y.-P. Ou, J. Zhang, M. Xu, J. Xia, F. Hartl, J. Yin, G.-A. Yu, S. H. Liu, *Chem. Asian J.* **2014**, *9*, 1152–1160.
- [65] S. Roue, H. Sahnoune, L. Toupet, J.-F. Halet, C. Lapinte, *Organometallics* **2016**, *35*, 2057–2070.
- [66] A. Arnanz, M.-L. Marcos, C. Moreno, D. H. Farrar, A. J. Lough, J. O. Yu, S. Delgado, J. Gonzalez-Velasco, *J. Organomet. Chem.* **2004**, *689*, 3218–3231.
- [67] S. Roue, S. Le Stang, L. Toupet, C. Lapinte, *C. R. Chim.* **2003**, *6*, 353–366.
- [68] P. Li, B. Ahrens, K.-H. Choi, M. S. Khan, P. R. Raithby, P. J. Wilson, W. Y. Wong, *CrystEngComm* **2002**, *4*, 405–412.
- [69] S. Le Stang, F. Paul, C. Lapinte, *Organometallics* **2000**, *19*, 1035–1043.
- [70] J. Lewis, N. J. Long, P. R. Raithby, G. P. Shields, W. Y. Wong, M. Younus, *J. Chem. Soc. Dalton Trans.* **1997**, 4283–4288.
- [71] E. Viola, C. Lo Sterzo, F. Trezzi, *Organometallics* **1996**, *15*, 4352–4354.
- [72] E. Viola, C. Lo Sterzo, R. Crescenzi, G. Frachey, *J. Organomet. Chem.* **1995**, *493*, C9–C13.
- [73] J. M. Speck, M. Korb, T. Rüffer, A. Hildebrandt, H. Lang, *Organometallics* **2014**, *33*, 4813–4823.
- [74] S. Roue, C. Lapinte, *J. Organomet. Chem.* **2005**, *690*, 594–604.
- [75] F. Lissel, O. Blacque, K. Venkatesan, H. Berke, *Organometallics* **2015**, *34*, 408–418.
- [76] Y.-P. Ou, J. Xia, J. Zhang, M. Xu, J. Yin, G.-A. Yu, S. H. Liu, *Chem. Asian J.* **2013**, *8*, 2023–2032.

- [77] M. I. Bruce, J. Davy, B. C. Hall, Y. J. V. Galen, B. W. Skelton, A. H. White, *Appl. Organomet. Chem.* **2002**, *16*, 559–568.
- [78] D. Beljonne, M. C. B. Colbert, P. R. Raithby, R. H. Friend, J. L. Bredas, *Synth. Met.* **1996**, *81*, 179–183.
- [79] N. Chawdhury, A. Kohler, R. H. Friend, M. Younus, N. J. Long, P. R. Raithby, J. Lewis, *Macromolecules* **1998**, *31*, 722–727.
- [80] N. Chawdhury, M. Younus, P. R. Raithby, J. Lewis, R. H. Friend, *Opt. Mater.* **1998**, *9*, 498–501.
- [81] M. Younus, A. Kohler, S. Cron, N. Chawdhury, M. R. A. Al-Mandhary, M. S. Khan, J. Lewis, N. J. Long, R. H. Friend, P. R. Raithby, *Angew. Chem. Int. Ed.* **1998**, *37*, 3036–3039.
- [82] N. Chawdhury, A. Kohler, R. H. Friend, W. Y. Wong, J. Lewis, M. Younus, P. R. Raithby, T. C. Corcoran, M. R. A. Al-Mandhary, M. S. Khan, *J. Chem. Phys.* **1999**, *110*, 4963–4970.
- [83] T. Yamamoto, T. Morikita, T. Maruyama, K. Kubota, M. Katada, *Macromolecules* **1997**, *30*, 5390–5396.
- [84] O. Gidron, Y. Diskin-Posner, M. Bendikov, *Chem. Eur. J.* **2013**, *19*, 13140–13150.
- [85] U. Pfaff, A. Hildebrandt, M. Korb, D. Schaarschmidt, M. Rosenkranz, A. Popov, H. Lang, *Organometallics* **2015**, *34*, 2826–2840.
- [86] U. Pfaff, A. Hildebrandt, M. Korb, S. Oßwald, M. Linseis, K. Schreiter, S. Spange, R. F. Winter, H. Lang, *Chem. Eur. J.* **2016**, *22*, 783–801.
- [87] Y. Tanaka, T. Ishisaka, T. Koike, M. Akita, *Polyhedron* **2015**, *86*, 105–110.
- [88] U. Pfaff, A. Hildebrandt, M. Korb, H. Lang, *Polyhedron* **2015**, *86*, 2–9.
- [89] A. K. Mahrok, E. I. Carrera, A. J. Tilley, S. Ye, D. S. Seferos, *Chem. Commun.* **2015**, *51*, 5475–5478.
- [90] A. C. Jahnke, M. Spulber, M. Neuburger, C. G. Palivan, O. S. Wenger, *Chem. Commun.* **2014**, *50*, 10883–10886.
- [91] D. M. D'Alessandro, A. C. Topley, M. S. Davies, F. R. Keene, *Chem. Eur. J.* **2006**, *12*, 4873–4884.
- [92] T. Ito, T. Hamaguchi, H. Nagino, T. Yamaguchi, J. Washington, C. P. Kubiak, *Science* **1997**, *277*, 660–663.
- [93] C. G. Atwood, W. E. Geiger, *J. Am. Chem. Soc.* **2000**, *122*, 5477–5485.
- [94] T. Ito, N. Imai, T. Yamaguchi, T. Hamaguchi, C. H. Londergan, C. P. Kubiak, *Angew. Chem. Int. Ed.* **2004**, *43*, 1376–1381.
- [95] P. Mücke, M. Linseis, S. Zálíš, R. F. Winter, *Inorg. Chim. Acta* **2011**, *374*, 36–50.
- [96] J. Maurer, B. Sarkar, B. Schwederski, W. Kaim, R. F. Winter, S. Zálíš, *Organometallics* **2006**, *25*, 3701–3712.
- [97] J. Maurer, B. Sarkar, W. Kaim, R. F. Winter, S. Zálíš, *Chem. Eur. J.* **2007**, *13*, 10257–10272.
- [98] J. Maurer, M. Linseis, B. Sarkar, B. Schwederski, M. Niemeyer, W. Kaim, S. Zálíš, C. Anson, M. Zabel, R. F. Winter, *J. Am. Chem. Soc.* **2008**, *130*, 259–268.
- [99] D. D. Kong, L. S. Xue, R. Jang, B. Liu, X. G. Meng, S. Jin, Y.-P. Ou, X. Hao, S. H. Liu, *Chem. Eur. J.* **2015**, *21*, 9895–9904.
- [100] A. Katritzky, C. Ramsden, J. Joule, V. Zhdankin, *Handbook of Heterocyclic Chemistry*, **2010**.
- [101] E. C. James, M. Jura, G. Kociok-Köhn, P. R. Raithby, E. L. Sharp, P. J. Wilson, *Inorg. Chem.* **2007**, *46*, 7232–7234.
- [102] S. H. Choi, I. Bytheway, Z. Lin, G. Jia, *Organometallics* **1998**, *17*, 3974–3980.

- [103] R. Taylor, *Cryst. Growth Des.* **2016**, *16*, 4165–4168.
- [104] C. B. Aakeröy, T. A. Evans, K. R. Seddon, I. Pálinkó, *New J. Chem.* **1999**, *23*, 145–152.
- [105] C. W. Bird, *Tetrahedron* **1985**, *41*, 1409–1414.
- [106] D. M. D'Alessandro, F. R. Keene, *Dalton Trans.* **2004**, 3950–3954.
- [107] A. O. Patil, A. J. Heeger, F. Wudl, *Chem. Rev.* **1988**, *88*, 183–200.
- [108] J. C. Salsman, C. P. Kubiak, T. Ito, *J. Am. Chem. Soc.* **2005**, *127*, 2382–2383.
- [109] T. Yamaguchi, N. Imai, T. Ito, C. P. Kubiak, *Bull. Chem. Soc. Jpn.* **2000**, *73*, 1205–1212.
- [110] A. P. Scott, L. Radom, *J. Phys. Chem.* **1996**, *100*, 16502–16513.
- [111] M. Renz, M. Kess, M. Diedenhofen, A. Klamt, M. Kaupp, *J. Chem. Theory Comput.* **2012**, *8*, 4189–4203.
- [112] M. Kaupp, M. Renz, M. Parthey, M. Stolte, F. Würthner, C. Lambert, *Phys. Chem. Chem. Phys.* **2011**, *13*, 16973–16986.
- [113] M. Kaupp, A. Karton, F. A. Bischoff, *J. Chem. Theory Comput.* **2016**, *12*, 3796–3806.
- [114] M. Kaupp, S. Gückel, M. Renz, S. Klawohn, K. Theilacker, M. Parthey, C. Lambert, *J. Comp. Chem.* **2016**, *37*, 93–102.
- [115] M. Kaupp, S. Gückel, M. Renz, S. Klawohn, K. Theilacker, M. Parthey, C. Lambert, *J. Comp. Chem.* **2015**, *37*, 93–102.
- [116] S. Marqués-González, M. Parthey, D. S. Yufit, J. A. K. Howard, M. Kaupp, P. J. Low, *Organometallics* **2014**, *33*, 4947–4963.
- [117] M. Parthey, K. B. Vincent, M. Renz, P. A. Schauer, D. S. Yufit, J. A. K. Howard, M. Kaupp, P. J. Low, *Inorg. Chem.* **2014**, *53*, 1544–1554.
- [118] M. Renz, M. Kaupp, *J. Phys. Chem. A* **2012**, *116*, 10629–10637.
- [119] M. Renz, K. Theilacker, C. Lambert, M. Kaupp, *J. Am. Chem. Soc.* **2009**, *131*, 16292–16302.
- [120] N. Ahmad, J. J. Levison, S. D. Robinson, M. F. Uttley, E. R. Wonchoba, G. W. Parshall, *Complexes of Ruthenium, Osmium, Rhodium, and Iridium Containing Hydride Carbonyl, or Nitrosyl Ligands*, John Wiley & Sons, Inc., **1974**.
- [121] D. P. Sweat, C. E. Stephens, *J. Organomet. Chem.* **2008**, *693*, 2463–2464.
- [122] J. D. Prugh, A. C. Huitric, W. C. McCarthy, *J. Org. Chem.* **1964**, *29*, 1991–1994.
- [123] S. Haid, A. Mishra, C. Urich, M. Pfeiffer, P. Bäuerle, *Chem. Mater.* **2011**, *23*, 4435–4444.
- [124] M. Krejčík, M. Daněk, F. J. Hartl, *J. Electroanal. Chem.* **1991**, *317*, 179–187.
- [125] M. J. Frisch, G. W. Trucks, H. B. Schlegel, G. E. Scuseria, M. A. Robb, J. R. Cheeseman, G. Scalmani, V. Barone, G. A. Petersson, H. Nakatsuji, et al., *Gaussian 09, Revision a*, Gaussian, Inc., **2009**.
- [126] P. J. Hay, W. R. Wadt, *J. Chem. Phys.* **1985**, *82*, 299–310.
- [127] W. R. Wadt, P. J. Hay, *J. Chem. Phys.* **1985**, *82*, 284–298.
- [128] P. J. Hay, W. R. Wadt, *J. Chem. Phys.* **1985**, *82*, 270–283.
- [129] G. A. Petersson, M. A. Al-Laham, *J. Chem. Phys.* **1991**, *94*, 6081–6090.
- [130] N. M. O'Boyle, A. L. Tenderholt, K. M. Langner, *J. Comp. Chem.* **2008**, *29*, 839–845.